Strain distribution in the proximal Human femur during in vitro simulated sideways fall

J Biomech. 2015 Jul 16;48(10):2130-43. doi: 10.1016/j.jbiomech.2015.02.022. Epub 2015 Mar 20.

Strain distribution in the proximal Human femur during in vitro simulated sideways fall

Lorenzo Zani, Paolo Erani, Lorenzo Grassi, Fulvia Taddei, Luca Cristofolini

PMID: 25843261

Strain distribution in the proximal human femur during *in vitro* simulated sideways fall

Lorenzo Zani, BEng[1], Paolo Erani, BEng[1], Lorenzo Grassi, MEng[1], Fulvia Taddei, PhD[1], Luca Cristofolini, PhD[2]

[1] Laboratorio di Tecnologia Medica, Istituto Ortopedico Rizzoli, Bologna, Italy

[2] Department of Industrial Engineering, School of Engineering and Architecture, University of Bologna, Italy

Submitted to: **J. Biomechanics (BM-D-14-01045)**
Version.0: 20th October 2014
Version.1: 7th January 2015
Version.2: 4th February 2015

Statistics:

Word count (manuscript):	3978 (Introduction to acknowledgements, excluding references, captions and tables)
Word count (abstract):	249 words
Figures:	9
Tables:	2
References:	56

Corresponding author:
Luca Cristofolini
Department of Industrial Engineering
School of Engineering and Architecture
University of Bologna
Viale Risorgimento, 2
40136 Bologna, Italy
E-mail: luca.cristofolini@unibo.it

ABSTRACT

This study assessed: (i) how the magnitude and direction of principal strains vary for different sideways fall loading directions; (ii) how the principal strains for a sideways fall differ from physiological loading directions; (iii) the fracture mechanism during a sideways fall. Eleven human femurs were instrumented with 16 triaxial strain gauges each. The femurs were non-destructively subjected to: (a) six loading configurations covering the range of physiological loading directions; (b) twelve configurations simulating sideways falls. The femurs were eventually fractured in a sideways fall configuration while high-speed cameras recorded the event. When the same force magnitude was applied, strains were significantly larger in a sideways fall than for physiological loading directions (principal compressive strain was 70% larger in a sideways fall). Also the compressive-to-tensile strain ratio was different: for physiological loading the largest compressive strain was only 30% larger than the largest tensile strain; but for the sideways fall, compressive strains were twice as large as the tensile strains. Principal strains during a sideways fall were nearly perpendicular to the direction of principal strains for physiological loading. In the most critical regions (medial part of the head-neck) the direction of principal strain varied by less than 9° between the different physiological loading conditions, whereas it varied by up to 17° between the sideways fall loading conditions. This was associated with a specific fracture mechanism during sideways fall, where failure initiated on the superior-lateral side (compression) followed by later failure of the medially (tension), often exhibiting a two-peak force-displacement curve.

Keywords: hip fractures, sideways fall, physiological loading, strain distribution, direction of principal strain, structural optimization

1. INTRODUCTION

Hip fractures represent a social burden causing more disability than any other type of fragility fractures (Cummings and Melton,2002; Rockwood et al.,1991; WHO,2007). The vast majority of hip fractures (nearly 90%) is a consequence of falls (Greenspan et al.,1994; Hayes et al.,1993). Therefore, understanding the mechanical response of the proximal femur to such overloading conditions is of fundamental importance.

There is a general agreement on the mechanism leading to fractures during falls: in most cases, the subject falls on his/her side, impacting the ground with the posterior-lateral side of the hip. Consequently, a force more or less perpendicular to the long axis of the femur (Laing and Robinovitch,2010; Nankaku et al.,2005) is delivered to the greater trochanter through the soft tissues. Several works experimentally investigated (e.g.: (Courtney et al.,1995; Eckstein et al.,2004; Lochmuller et al.,2003; Manske et al.,2008)) the strength of the human femur for a sideways fall loading conditions, starting from the '50s (Backman, 1957). It has been demonstrated (Keyak,2000) that the strength of the femur in sustaining the loads arising from a sideways fall is significantly lower than from physiological loading conditions (such as stance or walking). It is known (Pinilla et al.,1996) that this strength is highly influenced by the impact direction. However, a complete understanding of the mechanical response of the human femur to this accidental overloading condition is still lacking.

As falling itself is an unpredictable event, the direction of this force is unpredictable and can vary significantly between different falls. The first *in vitro* simulation of sideways fall loading of the femur is due to Backman (Backman, 1957): the femur was

internally rotated by 15°, and adducted by 10°. This loading configuration was replicated by others (e.g.: (Courtney et al.,1995; Eckstein et al.,2004; Lochmuller et al.,2003; Manske et al.,2008)), without a specific demonstration of the relevance of this (or any other) loading direction. The sensitivity of the failure load to the direction of the applied force has been assessed in vitro (Pinilla et al.,1996). Unfortunately, in that study the strain distribution was not investigated.

The strain distribution in the proximal femur has been extensively investigated *in vitro*, but mainly under simulated single-leg-stance (Cristofolini,1997; Cristofolini et al.,2010; Cristofolini et al.,2009; Fung,1980; Huiskes et al.,1981). The strain distribution in the femur for a simulated fall was first measured by (Lotz et al.,1991); however, the sample size and the tested conditions were limited (one femur, with 9 strain gauges, subjected to one loading configuration: internally rotated by 30° and adducted by 30°). More recently, a combined experimental-numerical study was based on three femurs prepared with 16 triaxial strain gauges (Grassi et al.,2012). Recent studies with digital image correlation (Gilchrist et al.,2014; Helgason et al.,2014) again simulated a single fall loading configuration (15° internal rotation, 10° adduction). A numerical study (Majumder et al.,2009) analyzed the sensitivity of the strain distribution to the direction of the applied forces but still on a single specimen.

The fracture mechanism has recently been elucidated for para-physiological loads by means of high-speed videos (Cristofolini et al.,2007) and other high-speed techniques for fracture assessment (Juszczyk et al.,2010; Juszczyk et al.,2013; Juszczyk et al.,2011). The fracture mechanism during a sideways falls was investigated *in vitro* with high-speed cameras (de Bakker et al.,2009). However, in this study the strain distribution was not investigated. To the authors' knowledge a

systematic investigation of the mechanical response (including the magnitude and alignment of tensile and compressive strains) of the proximal femur to sideways fall loading conditions, and its variability with respect to different but plausible loading directions, has never been presented.

The aim of the present work was to analyze the mechanical behaviour of the proximal femur for the non-physiologic loading condition occurring in sideways falls, by means of experimental tests on human femurs. More specifically, this study assessed how the magnitude and direction of principal strains varied for a range of physiological and sideways fall loading directions, and investigated the fracture mechanism during sideways fall.

2. MATERIALS AND METHODS

2.1 Overview

Human femurs were instrumented with strain gauges, and tested non-destructively in different loading configurations that replicated: (i) a range of physiological loading directions; (ii) a range of possible loading directions during a sideways fall. Each specimen was eventually tested to failure in a sideways fall configuration while high-speed videos were acquired.

2.2 Preparation of test specimens

Eleven fresh-frozen femurs (Table 1) from eight donors who did not suffer from cancer or musculoskeletal pathologies (other than osteoporosis) were obtained through an ethically-approved international donation program (http://www.iiam.org/). Bone quality and lack of defects were verified through Dual-energy X-ray absorptiometry (DXA: Eclipse, Norland Co., USA), and computed tomography scanning (CT: Hi-Speed, General Electric, USA). The femurs were wrapped in cloths soaked with physiological solution during the whole procedure to avoid dehydration, and stored at -20°C when not in use. Biomechanical length (BL) and diameter of the head (HD) were measured as in (Cristofolini et al.,2009). An anatomical reference frame was marked on each femur (Cristofolini,2012). After resecting the condyles, the distal end of each specimen was embedded in acrylic bone cement in an aluminum pot (100-mm deep) so that 33% of the biomechanical length was free (Fig. 1).

2.3 Strain measurements

Each femur was instrumented with triaxial-stacked strain gauges at 16 locations as in (Zani et al.,2014) (Fig. 1). The area for strain measurement was prepared following

109 an established procedure for wet cadaveric specimens (Cristofolini et al.,2010;
110 Viceconti et al.,1992). Both 0.8-mm grid (C2A-06-031WW-350, Vishay Micro-
111 Measurement, Pennsylvania, USA) and 2-mm grid (KFW-2-120-D17-11 L5M2S,
112 Kiowa Electronic Instruments, Tokyo, Japan) were used, depending on the space
113 available. To prevent bone surface heating, a grid excitation of 0.5 V was selected.
114 During both non-destructive and destructive tests, strains were sampled at 2 kHz using
115 a multi-channel data logger (System 6000, Vishay Micro-Measurement, USA),
116 synchronously with the signals from the testing machine. To prevent aliasing, and
117 eliminate mechanical and electrical noise, all signals were low-pass filtered with six-
118 pole Butterworth filter (cut-off: 50 Hz).

119 **2.4 *In vitro* non-destructive test: physiological loading**

120 A single force was applied by the testing machine (Mod. 8502, Instron, Canton, MA,
121 USA) to the femoral head along different directions. Six loading configurations (LCs)
122 were evaluated (Cristofolini et al.,2009) (Fig. 2). LC1-4 corresponded to the extreme
123 angles of the resultant force acting at the hip joint in the frontal and sagittal planes
124 during different physiological motor tasks (Bergmann et al.,2001). LC5 is frequently
125 used in the literature and replicates a simplified single-leg-stance
126 (Lochmüller et al.,2002) in which the force was parallel to the femoral diaphysis.
127 LC6 has been proposed to reproduce spontaneous fractures (Cristofolini et al.,2007):
128 an angle of 8° in the frontal plane has been shown to induce the highest stresses in the
129 proximal femoral metaphysis (Taddei et al.,2006). A force of 0.75 of the donor's
130 body weight (BW) was applied for all loading configurations to prevent bone damage.
131 The actuator speed (displacement control, linear ramp) was tuned for each specimen
132 based on preliminary tests, so that full-load was reached in 0.2 seconds. This is the

typical timescale of physiological and para-physiological loading (Bergmann et al.,2004), and has been proposed for *in vitro* testing (Cristofolini et al.,2010; Cristofolini et al.,2009; Raftopoulos et al.,1993). The full-load position was held for 0.2 seconds before unloading. Each configuration was repeated six times on each specimen, with a recovery time of 5 minutes between repetitions to ensure the absence of any residual strains (Cristofolini et al.,2010).

2.5 *In vitro* non-destructive test: sideways fall

A validated setup (Zani et al.,2014) allowed testing the same specimen with different loading directions, while avoiding any over-constraint by means of low-friction bearings (Fig. 3). A force was applied by the actuator of the testing machine to the femoral head while the specimen was constrained distally (free to tilt in a vertical plane, medial side up). The greater trochanter rested on a sliding flat support. To reduce the risk of local crushing, the head and trochanter were protected with custom-machined aluminum spherical caps fixed with bone cement.

Three values were selected for the internal rotation (0°, 15°, 30°), and four for the adduction angle (0°, 10°, 20°, 30°). All 12 combinations (4x3 full-factorial scheme) were applied to all specimens, including the classical configuration: 15° internal rotation, 10° adduction (Backman, 1957).

Similar to the physiological loading configurations, a force of 0.75 BW was applied to the femoral head in 0.2 seconds (position control, linear ramp, with a suitable specimen-dependent actuator speed); full-load position was held for 0.2 seconds before unloading. Each configuration was repeated six times, with a recovery of 5 minutes.

2.6 *In vitro* destructive test: sideways fall loading

To supplement the strain distributions measured non-destructively, the femurs were eventually tested to failure. Consistent with the literature (Backman, 1957), destructive tests were conducted at 15° internal rotation – 10° adduction with a single monotonic ramp up to macroscopic failure. A study on volunteers has shown that the force peak is reached in a time of the order of 0.1 seconds (Laing and Robinovitch,2010). The optimal actuator speed to achieve fracture in approximately 0.1 seconds was estimated for each specimen, based on the non-destructive testing (scaling to an estimated failure strain of -10000 and +7000 microstrain (Bayraktar et al.,2004)). This resulted in an actuator speed between 15 and 50 mm/second. (Table 2) This is within the published range (2-100 mm/sec (Bouxsein et al.,1999; Pinilla et al.,1996)). All specimens eventually fractured in 0.09-0.17 seconds. This is slower than with drop-tower loading (average impact speed 114 mm/second; peak speed 3 m/second; failure in 0.02 seconds (Gilchrist et al.,2014)). Similar to the non-destructive testing, all signals (including strain gauges) were recorded at 2 kHz.

To fully document the mode of failure, the destructive tests were video-recorded using high-speed cameras (Fastcam SA1, SA3, or SA4 - depending on the test session - Photron, San Diego, CA, USA) at 10000-15000 frames per second, with a typical pixel size of 0.1-0.2 mm, following an established procedure (Cristofolini et al.,2007) (Fig. 3). The camera and two mirrors allowed recording three views of the specimen in the same frame. Three high-intensity light sources (1000W + 300W + 300W) were used, allowing optimal image sharpness due to short shutter times and high aperture setting.

2.7 Statistical methods

The Peirce criterion was applied to exclude outliers (Ross,2003). First, for each specimen, each loading configuration and each strain gauge, outliers were checked among repetitions: approximately 2.5% of the data was excluded. Repeatability (intra-specimen variability) was good: for the physiological loading the Coefficient of Variation between test repetitions was on average 0.4% (0.7% in the worst specimen); for the sideways fall, it was on average 0.5% (1.7% in the worst specimen). To obtain a single output for each strain gauge and each specimen, the average over six repetitions was calculated for the principal strains (ε_1, ε_2), and the angle (θ_p) of the principal strain. Finally, the Peirce criterion was applied among the 11 specimens: none of them was excluded.

The significance of variations of principal strains between loading configurations was assessed with Repeated-Measures ANOVA with one factor (LC1-LC6) for the physiological loading configurations, and with two factors (internal-rotation and adduction angles) for the simulated sideways fall.

To assess the effect of the different loading configurations on the direction of principal strains, the angle (θ_p) measured for the different loading configurations was referred to the value found (for the same specimen and same strain gauge) for the physiological loading at 8° in the frontal plane (LC6). As the angle of principal strain does not follow a normal distribution, the Kruskal-Wallis non-parametric test was applied separately for the physiological configurations, for the internal rotation, and the adduction angles of the sideways fall.

Statistical analyses were performed with StatView-5.0.1 (SAS-Institute, Cary, NC, USA).

3. RESULTS

3.1 Magnitude of principal strains

For the physiological loading configurations, the largest tensile strains were observed on the superior-lateral side, while compression dominated in the medial side. Peak compressive strains (maximum: -1102 microstrain) were larger than the tensile ones (maximum: +911 microstrain) in absolute value. Large variations of principal strains were observed between the six configurations (Fig. 4). In the head and neck region, such differences were generally highly significant (ANOVA, $p<0.05$) for the maximum tensile strain, but generally not for the compressive one. Only the medial side made an exception, as most differences were not significant.

With a simulated sideways fall, tension dominated on the medial side, compression on the superior-lateral side (Fig. 5). The largest absolute values were found in the head-neck region. Peak compressive strains (up to -1284 microstrain) were larger than the tensile ones (maximum: +680 microstrain) in absolute value. The variations of principal strains in relation to the internal rotation angle were large (significant at several locations in the head and neck region, ANOVA $p<0.05$, Fig. 5). Conversely, the adduction angle had generally a smaller effect, which was significant mainly on the medial and lateral sides (ANOVA $p>0.05$, Fig. 5).

3.2 Direction of principal strains

For the physiological loading, the direction of principal strains varied very little between the six configurations (Fig. 6): less than 18° in the most stressed parts (medial and superior-lateral sides of the head-neck region, Kruskal-Wallis $p>0.5$). The largest

225 rotations of the principal strain were observed for the most tilted loading
226 configurations (LC1,LC4).

227 With a simulated sideways fall, the direction of principal strain was nearly
228 perpendicular to that during physiological loading at all strain measurement locations
229 (Fig. 7). The direction of principal strain varied less in the head-neck region (range
230 23° over the 12 sideways fall loading directions) than in the distal region (where the
231 strain magnitude was significantly lower). The internal rotation angle had a large
232 effect on the direction of principal strains (significant at most locations in the head-
233 neck region, Kruskal-Wallis, $p<0.05$, Fig. 7). Conversely, the adduction angle had
234 generally a smaller effect (not significant in the entire head-neck region, Kruskal-
235 Wallis, $p>0.5$, Fig. 7), except in regions where the strain magnitude was small (e.g.
236 gauges A3, P3).

237 More details about the angle (θ_p) of the principal strain are reported in the
238 supplementary material <LINK>.

239 **3.3 Fracture mechanism**

240 The peak force recorded during the destructive tests ranged 1170-6525 N (1.57-7.31
241 BW, Table 2). Seven specimens exhibited a two-phase failure (Fig. 8): failure started
242 on the superior-lateral side of the head-neck region (compression), but complete failure
243 was achieved several milliseconds later, with cracking of the inferior-medial side
244 (tension). Similar failure patterns were observed for femurs from the same pair.
245 However, four specimens failed due to crushing of the greater trochanter (with no
246 proper neck fracture), which is different from the clinically-observable inter-

247 trochanteric fractures. The force-displacement curves and the high-speed videos are
248 available as supplementary material <LINK>.

249 The trend of strain over time was highly-linear up to failure in all specimens (Fig. 9).
250 During the destructive test, some strain gauges failed prior to femur fracture, either due
251 to excessive deformation of the grid material, or to local fracture of the underlying
252 bone. The largest tensile strains during the destructive tests were always found in the
253 medial gauges of the head-neck region (4000÷5000 microstrain at the force peak). The
254 largest compressive strains were always in the head-neck region, but location varied
255 between femurs (-6000÷ -8000 microstrain at the force peak).
256

4. DISCUSSION

The aim of this study was to investigate in detail the strain distribution in the proximal femur during a sideways fall. Therefore, we assessed how the magnitude and direction of principal strains varied for a range of possible sideways fall loading directions, and we compared them to those recorded during simulated physiological loading. Direct comparisons between the two types of loading were possible as the same 11 femurs were tested in both conditions. To elucidate how the strain distribution affects the mode of failure, we also investigated the fracture mechanism during sideways fall by means of high-speed video. Tension and compression were reversed in a simulated sideways fall compared to physiological loading; the ratio between compressive and tensile strain magnitudes was considerably higher for a sideways fall than for physiological loading.

Our study has shown that the largest strains during a sideways fall are localized in the head-neck region (Fig. 5), which is where fracture eventually occurs (Fig. 8). Increasing the internal rotation in the range 0-30°, and increasing the adduction angle in the range 0-30° caused a significant strain increase in this region. Such a loading direction can be associated with a postero-lateral fall, with the lower limb adducted and flexed (Majumder et al.,2009; Nankaku et al.,2005; van den Kroonenberg et al.,1995; van den Kroonenberg et al.,1996)

If a material has different behaviour in tension/compression, failure will occur either in the tensile/compressive area, depending on where the applied stress exceeds the tensile/compressive strength. Bone tissue is 40% stronger in compression than in tension (-10000 versus +7000 microstrain (Bayraktar et al.,2004)). For the physiological loading configurations, the largest compressive strain (gauge MN: -752 microstrain, average of 11 specimens) was only 30% larger in absolute value than the

largest tensile strain (LH: +509 microstrain). This could explain why fracture initiates on the superior-lateral side (largest tension) when para-physiological loads are applied *in vitro* (Cristofolini et al.,2007; Grassi et al.,2014; Juszczyk et al.,2011; Keyak et al.,2005), producing a similar fracture to what is observed for spontaneous fractures *in vivo* (Grisso et al.,1991; Rockwood et al.,1991; Yang et al.,1996). Conversely, with a simulated sideways fall, the largest compressive strain (gauge LN: -1284 microstrain, average of 11 specimens) was twice as large as the largest tensile strain (MN: +680 microstrain). Moreover, compressive strain (both average and peak) in a sideways fall was larger than for a physiological loading direction for the same force magnitude. This may explain why fracture during sideways fall initiates on the superior-lateral side due to compression (see Fig. 8 and (de Bakker et al.,2009)).

For physiological loading, we found that the direction of the principal tensile strain was generally aligned with the neck–diaphysis axis on the lateral side and was perpendicular on the medial side. For a sideways fall, the direction of principal strains was nearly perpendicular to that during physiological loading (supposedly the condition for which the femur structure is optimized (Cristofolini, IN PRESS)).

Our results concerning the principal strains and their direction for the physiological loading scenarios are well in agreement with a previous study on different specimens (Cristofolini et al.,2009). The direction of principal strains varied by a relatively small angle between physiological loading configurations. As strain measurements were performed when the applied force was tilted to cover the cone spanned by the hip joint resultant, this suggests that the principal strain directions vary little for most physiological motor tasks. Hence, the state of stress in the proximal metaphysis allows structural optimization (in terms of local tissue arrangement, and anisotropy) to face most physiological tasks. Conversely, when a sideways fall was simulated the

direction of principal strain varied by a larger angle in relation to the direction of the applied force, suggesting that the bone structure can hardly withstand such a loading direction. For instance, in the medial side of the head and neck (gauges MH, MN, Fig. 6-7) the direction of principal strain varied by less than 9° between the different physiological loading conditions, whereas it varied by up to 17° between the sideways fall loading conditions.

The failure force for a sideways fall in this study ranged 1170N-6525N (median: 2796N). A recent study, where 12 femurs were tested to failure in a para-physiological loading (Juszczyk et al.,2011), reported a higher failure force (range: 3740N-10502N, median 6712N), although the sample had lower bone quality (median t-score: -3.31) than the present sample (Table 1). Such a difference between the two loading scenarios is in agreement with the literature: the strength of the femur in a sideways fall is lower than for physiological loading by a factor between 2.16 according to an in vitro study (Keyak,2000), 2.85 according to a FE study (Keyak et al., 2001), 3.5 according to another *in vitro* study (Duchemin et al., 2006), and 4.4 according to another FE simulation (Bessho et al., 2009).

More in general, this confirms the concept of a structural optimization due to a combination of generational evolution, and local adaptation (Cristofolini, IN PRESS).

The two-phase failure pattern we observed is in agreement with (de Bakker et al.,2009; Gilchrist et al.,2014; Helgason et al.,2014) both in terms of points of initiation (compressive failure starts on the superior-lateral side, followed by tensile fracture on the medial side), and in terms of trend in the force-displacement curves.

An increase of the rotation angle from 0° to 30° was associated with a 24% decrease of the failure force (Pinilla et al.,1996). This is compatible with our results: in the superior-lateral neck region, the principal compressive strains were 10-12% larger at 30° than at 0° internal rotation, for the same 10° adduction angle (Fig. 5).

We should also account for some limitations of our work. Strain measurements during sideways fall in the lateral part of the diaphysis (gauge L1) were possibly perturbed by the presence of the aluminum cap on the greater trochanter. Furthermore, no soft tissue was present on the greater trochanter, which provides some padding *in vivo*. This is reflected by the unusual failure mechanism of the four specimens in which the greater trochanter got crushed, despite the aluminum caps.

The specimens included in this study were biased towards the elderly and osteoporotic. For this reason, our results might not be representative of the entire human population. However, as fractures in most cases occur in the elderly (Cummings and Melton,2002; Rockwood et al.,1991; WHO,2007), our sample is representative of this high-risk class of subjects. In all cases, our study excluded donors affected by cancer or other pathologies possibly compromising the musculoskeletal system (except osteoporosis).

We did not simulate any specific motor task for the physiological loading. Conversely, the six load cases simulated explored the entire range of possible loading directions during daily tasks (Bergmann et al.,2001; Cristofolini et al.,2010; Cristofolini et al.,2009).

For the sideways fall, as no direct measurement is available concerning the direction of the forces delivered in a real fall, we decided to explore a wide range of possible loading directions, using a validated setup (Zani et al.,2014). We preferred a displacement-control test, as opposed to a drop-tower system (Gilchrist et al.,2013;

Gilchrist et al.,2014; Helgason et al.,2014) to (i) have a better control of the test conditions, and (ii) to be able to test the same specimen repeatedly, under different loading conditions. The actuator speed (15-50 mm/second) was slower than the typical impact speed during fall, but it was suitable to fracture all femurs in 0.09-0.17 seconds (compared to ~0.02 seconds for drop-tower testing (Gilchrist et al.,2014; Helgason et al.,2014)) due to the absence of soft tissues interposed. It must also be noted that, while in a drop-tower test the actual speed and loading rate vary as a function of the nonlinear stiffness (similar to what happens in a real fall), in our test a constant actuator speed was imposed.

Muscle forces were not directly simulated in our study. For the physiological loading, it has been shown that femur deflection depends also on the local action of the muscle forces (Speirs et al.,2007). Conversely, using an FE model of a single femur, it has been shown that small differences existed between the principal tensile strain distributions on the surface of the head-neck region with and without muscle forces when the same resultant force was applied at the femoral head (Cristofolini et al.,2007). Not including the muscle forces was considered a conservative approach in terms of predicted fracture force for the head-neck region. This simplification does not apply to the inter-trochanteric region and the diaphysis, where the local effect of the muscles cannot be neglected. No reliable information is available concerning the level of contraction of the hip muscles during a real sideways fall.

Since 4 femurs out of 11 samples were paired (Table 1), the assumption of independent samples that underlies most statistical tests is partly compromised. As no dedicated test is available for partly inter-dependent samples, standard parametric and non-parametric tests were adopted.

A full-field strain analysis was performed by (Gilchrist et al.,2014; Helgason et al.,2014), but limited to the superior-lateral region, and for a single loading configuration. It is worth noting that the accurate description of the strains field in the proximal femur under a variety of loading conditions is fundamental in the validation of finite element models that can be used for the improvement of fracture risk prediction in clinical applications (Falcinelli et al.,2014). In our study, measurements were available at 16 locations, sampling the entire proximal femur, and for a variety of loading configurations. Part of the present results have already been used as a comprehensive validation benchmark for numerical models (Grassi et al.,2012; Schileo et al.,2014), but information on strain levels and orientations may be further exploited to corroborate models of bone anisotropy.

In conclusion, this study has provided detailed information about the magnitude and direction of compressive and tensile strains, and of the different compression-tension ratio for physiological loading and for a sideways fall, which has not been systematically studied in the past. These findings also help explain why the femur is significantly weaker in a sideways fall, and why fracture initiates in a different region compared to physiological loading.

Acknowledgments: The Authors wish to thank Marco Viceconti for the stimulating discussions and for inspiring this entire study; Mateusz Juszczyk, Perrine Maisin, Joana Araujo, Philip Pogrzeba for the technical support; Luigi Lena for the artwork. This study was partially funded by the European Community Seventh Framework Programme (''The Osteoporotic Virtual Physiological Human—VPHOP'' Grant FP7-ICT2008-223865, and ''MXL'', Grant ICT-2009.5.2 248693), and by the Italian Ministry of Education (PRIN 2010-11, Grant 2010R277FT "Fall risk estimation and prevention in the elderly using a quantitative multifactorial approach").

Conflict of interest statement: There is no potential conflict of interest: none of the Authors received or will receive direct or indirect benefits from third parties for the performance of this study.

REFERENCES

Backman, S., 1957. The proximal end of the femur: investigations with special reference to the etiology of femoral neck fractures; anatomical studies; roentgen projections; theoretical stress calculations; experimental production of fractures. Acta Radiol Suppl, 1-166.

Bayraktar, H.H., Morgan, E.F., Niebur, G.L., Morris, G.E., Wong, E.K., Keaveny, T.M., 2004. Comparison of the elastic and yield properties of human femoral trabecular and cortical bone tissue. J Biomech 37, 27-35.

Bergmann, G., Deuretzbacher, G., Heller, M., Graichen, F., Rohlmann, A., Strauss, J., Duda, G.N., 2001. Hip contact forces and gait patterns from routine activities. J Biomech 34, 859-871.

Bergmann, G., Graichen, F., Rohlmann, A., 2004. Hip contact forces during stumbling. Langenbecks Arch. Surg. 389, 51-59.

Bessho, M., Ohnishi, I., Matsumoto, T., Ohashi, S., Matsuyama, J., Tobita, K., Kaneko, M., Nakamura, K., 2009. Prediction of proximal femur strength using a CT-based nonlinear finite element method: differences in predicted fracture load and site with changing load and boundary conditions. Bone 45, 226-231.

Bouxsein, M.L., Coan, B.S., Lee, S.C., 1999. Prediction of the strength of the elderly proximal femur by bone mineral density and quantitative ultrasound measurements of the heel and tibia. Bone 25, 49-54.

Courtney, A.C., Wachtel, E.F., Myers, E.R., Hayes, W.C., 1995. Age-related reductions in the strength of the femur tested in a fall-loading configuration. J Bone Joint Surg Am 77, 387-395.

Cristofolini, L., 1997. A critical analysis of stress shielding evaluation of hip prostheses. Critical Reviews in Biomedical Engineering 25:4&5, 409-483.

Cristofolini, L., 2012. Anatomical reference frames for long bones: biomechanical applications, in: Preedy, V.R. (Ed.), Handbook of Anthropometry: Physical Measures of Human Form in Health and Disease. Springer, New York.

Cristofolini, L., IN PRESS. In vitro evidence of the structural optimization of the human skeletal bones. J Biomechanics.

Cristofolini, L., Conti, G., Juszczyk, M., Cremonini, S., Van Sint Jan, S., Viceconti, M., 2010. Structural behaviour and strain distribution of the long bones of the human lower limbs. J Biomechanics 43, 826-835.

441 Cristofolini, L., Juszczyk, M., Martelli, S., Taddei, F., Viceconti, M., 2007. In vitro
442 replication of spontaneous fractures of the proximal human femur. J. Biomechanics 40,
443 2837-2845.

444 Cristofolini, L., Juszczyk, M., Taddei, F., Viceconti, M., 2009. Strain distribution in
445 the proximal human femoral metaphysis. Proc Inst Mech Eng [H] 223, 273-288.

446 Cummings, S.R., Melton, L.J., 2002. Epidemiology and outcomes of osteoporotic
447 fractures. Lancet 359, 1761-1767.

448 de Bakker, P.M., Manske, S.L., Ebacher, V., Oxland, T.R., Cripton, P.A., Guy, P.,
449 2009. During sideways falls proximal femur fractures initiate in the superolateral
450 cortex: evidence from high-speed video of simulated fractures. J Biomech 42, 1917-
451 1925.

452 Duchemin, L., Skalli, W., Topouchian, V., Benissa, M., Mitton, D., 2006, Femoral
453 fracture load and failure energy in two load configurations: an in vitro study. In 16th
454 EORS Annual meeting. Bologna.

455 Eckstein, F., Wunderer, C., Boehm, H., Kuhn, V., Priemel, M., Link, T.M.,
456 Lochmüller, E.-M., 2004. Reproducibility and side differences of mechanical tests for
457 determining the structural strength of the proximal femur. J. Bone and Mineral
458 Research 19, 379-385.

459 Falcinelli, C., Schileo, E., Balistreri, L., Baruffaldi, F., Bordini, B., Viceconti, M.,
460 Albisinni, U., Ceccarelli, F., Milandri, L., Toni, A., Taddei, F., 2014. Multiple loading
461 conditions analysis can improve the association between finite element bone strength
462 estimates and proximal femur fractures: a preliminary study in elderly women. Bone
463 67, 71-80.

464 Fung, Y.C., 1980. Bone and cartilage, Biomechanics - Mechanical properties of living
465 tissues. Springer Verlag, New York, pp. 383-415.

466 Gilchrist, S., Guy, P., Cripton, P.A., 2013. Development of an inertia-driven model of
467 sideways fall for detailed study of femur fracture mechanics. J Biomech Eng 135,
468 121001.

469 Gilchrist, S., Nishiyama, K.K., de Bakker, P., Guy, P., Boyd, S.K., Oxland, T.,
470 Cripton, P.A., 2014. Proximal femur elastic behaviour is the same in impact and
471 constant displacement rate fall simulation. Journal of Biomechanics 47, 3744-3749.

472 Grassi, L., Schileo, E., Taddei, F., Zani, L., Juszczyk, M., Cristofolini, L., Viceconti,
473 M., 2012. Accuracy of finite element predictions in sideways load configurations for
474 the proximal human femur. J Biomech 45, 394-399.

475 Grassi, L., Vaananen, S.P., Amin Yavari, S., Jurvelin, J.S., Weinans, H., Ristinmaa,
476 M., Zadpoor, A.A., Isaksson, H., 2014. Full-field strain measurement during
477 mechanical testing of the human femur at physiologically relevant strain rates. J
478 Biomech Eng 136.

479 Greenspan, S.L., Myers, E.R., Maitland, L.A., Resnick, N.M., Hayes, W.C., 1994. Fall
480 severity and bone mineral density as risk factors for hip fracture in ambulatory elderly.
481 Jama 271, 128-133.

482 Grisso, J.A., Kelsey, J.L., Strom, B.L., Chiu, G.Y., Maislin, G., O'Brien, L.A.,
483 Hoffman, S., Kaplan, F., 1991. Risk factors for falls as a cause of hip fracture in
484 women. The Northeast Hip Fracture Study Group. N. Engl. J. Med. 324, 1326-1331.

485 Hayes, W.C., Myers, E.R., Morris, J.N., Gerhart, T.N., Yett, H.S., Lipsitz, L.A., 1993.
486 Impact near the hip dominates fracture risk in elderly nursing home residents who fall.
487 Calcif Tissue Int 52, 192-198.

488 Helgason, B., Gilchrist, S., Ariza, O., Chak, J.D., Zheng, G., Widmer, R.P., Ferguson,
489 S.J., Guy, P., Cripton, P.A., 2014. Development of a balanced experimental-
490 computational approach to understanding the mechanics of proximal femur fractures.
491 Med Eng Phys 36, 793-799.

492 Huiskes, R., Janssen, J.D., Sloof, T.J., 1981. A detailed comparison of experimental
493 and theoretical stress-analyses of a human femur, in: Cowin, S.C. (Ed.), Mechanical
494 properties of bone. A.S.M.E., New York, pp. 211-234.

495 Juszczyk, M., Cristofolini, L., Kaniuk, J., Schileo, E., Viceconti, M., 2010. A novel
496 method for determining the time and location of abrupt fracture initiation in bones. J.
497 Strain Analysis in Engineering Design 45, 481-493.

498 Juszczyk, M.M., Cristofolini, L., Salvà, M., Zani, L., Schileo, E., Viceconti, M., 2013.
499 Accurate in vitro identification of fracture onset in bones: Failure mechanism of the
500 proximal human femur. J Biomechanics 46, 158-164.

501 Juszczyk, M.M., Cristofolini, L., Viceconti, M., 2011. The human proximal femur
502 behaves linearly elastic up to failure. J Biomech 44, 2259-2266.

503 Keyak, J.H., 2000. Relationships between femoral fracture loads for two load
504 configurations. J Biomech. 33, 499-502.

505 Keyak, J.H., Skinner, H.B., Fleming, J.A., 2001. Effect of force direction on femoral
506 fracture load for two types of loading conditions. J Orthop Res 19, 539-544.

507 Keyak, J.H., Kaneko, T.S., Tehranzadeh, J., Skinner, H.B., 2005. Predicting proximal
508 femoral strength using structural engineering models. Clin Orthop Relat Res, 219-228.

509 Laing, A.C., Robinovitch, S.N., 2010. Characterizing the effective stiffness of the
510 pelvis during sideways falls on the hip. Journal of Biomechanics 43, 1898-1904.

511 Lochmüller, E.-M., Groll, O., Kuhn, V., Eckstein, F., 2002. Mechanical strength of the
512 proximal femur as predicted from geometric and densitometric bone properties at the
513 lower limb versus the distal radius. Bone 30, 207-216.

514 Lochmuller, E.M., Muller, R., Kuhn, V., Lill, C.A., Eckstein, F., 2003. Can novel
515 clinical densitometric techniques replace or improve DXA in predicting bone strength
516 in osteoporosis at the hip and other skeletal sites? J Bone Miner Res 18, 906-912.

517 Lotz, J.C., Cheal, E.J., Hayes, W.C., 1991. Fracture prediction for the proximal femur
518 using finite element models: Part I--Linear analysis. J Biomech Eng 113, 353-360.

519 Majumder, S., Roychowdhury, A., Pal, S., 2009. Effects of body configuration on
520 pelvic injury in backward fall simulation using 3D finite element models of pelvis-
521 femur-soft tissue complex. Journal of biomechanics 42, 1475-1482.

522 Manske, S.L., Liu-Ambrose, T., Cooper, D.M., Kontulainen, S., Guy, P., Forster, B.B.,
523 McKay, H.A., 2008. Cortical and trabecular bone in the femoral neck both contribute
524 to proximal femur failure load prediction. Osteoporos Int.

525 Nankaku, M., Kanzaki, H., Tsuboyama, T., Nakamura, T., 2005. Evaluation of hip
526 fracture risk in relation to fall direction. Osteoporos Int 16, 1315-1320.

527 Pinilla, T.P., Boardman, K.C., Bouxsein, M.L., Myers, E.R., Hayes, W.C., 1996.
528 Impact direction from a fall influences the failure load of the proximal femur as much
529 as age-related bone loss. Calcif Tissue Int 58, 231-235.

530 Raftopoulos, D., Katsamanis, E., Saul, F., Liu, W., Saddemi, S., 1993. An intermediate
531 loading rate technique for the determination of mechanical properties of human
532 femoral cortical bone. J. Biomed. Eng. 15, 60-66.

533 Rockwood, C.A.J., Green, D.P., Bucholz, R.W., 1991. Rockwood and Green's
534 fractures in adults, 3 ed. J.B. Lippincott, Philadelphia.

535 Ross, S.M., 2003. Peirce's criterion for the elimination of suspect exerimental data.
536 Journal of Engineering Technology; Fall 2003 20, 38-48.

537 Ruff, C.B., Hayes, W.C., 1983. Cross-sectional Geometry of Pecos Pueblo Femora and
538 Tibiae - A Biomechanical Investigation: I. Method and General Patterns of Variation.
539 Am. J. Phys. Anthropol. 60, 359-381.

540 Schileo, E., Balistreri, L., Grassi, L., Cristofolini, L., Taddei, F., 2014. To what extent
541 can linear finite element models of human femora predict failure under stance and fall
542 loading configurations? J Biomech 47, 3531-3538.

543 Speirs, A.D., Heller, M.O., Duda, G.N., Taylor, W.R., 2007. Physiologically based
544 boundary conditions in finite element modelling. J Biomech 40, 2318-2323.

545 Taddei, F., Cristofolini, L., Martelli, S., Gill, H.S., Viceconti, M., 2006. Subject-
546 specific finite element models of long bones: An in vitro evaluation of the overall
547 accuracy. J Biomech 39, 2457-2467.

548 Taddei, F., Palmadori, I., Taylor, W.R., Heller, M.O., Bordini, B., Toni, A., Schileo,
549 E., 2014. European Society of Biomechanics S.M. Perren Award 2014: Safety factor
550 of the proximal femur during gait: A population-based finite element study. J Biomech
551 47, 3433-3440.

552 van den Kroonenberg, A.J., Hayes, W.C., McMahon, T.A., 1995. Dynamic models for
553 sideways falls from standing height. J Biomech Eng 117, 309-318.

554 van den Kroonenberg, A.J., Hayes, W.C., McMahon, T.A., 1996. Hip impact velocities
555 and body configurations for voluntary falls from standing height. Journal of
556 biomechanics 29, 807-811.

557 Viceconti, M., Toni, A., Giunti, A., 1992. Strain gauge analysis of hard tissues: factors
558 influencing measurements, in: Little, E.G. (Ed.), Experimental Mechanics. Technology
559 transfer between high tech engineering and biomechanics. Elsevier Science Publisher
560 B.V., Amsterdam, pp. 177-184.

561 WHO, 2007. Scientific group on the assessment of osteoporosis at primary health care
562 level (report of the World Health Organization:
563 http://www.who.int/chp/topics/Osteoporosis.pdf), p. 17.

564 Yang, K.-H.-., Shen, K.L., Demetropoulos, C.K., King, A.I., Kolodziej, P., Levine,
565 R.S., Fitzgerald, R.H.J., 1996. The relationship between loading conditions and
566 fracture patterns of the proximal femur. J. Biomech. Eng. 118, 575-578.

567 Zani, L., Cristofolini, L., Juszczyk, M.M., Grassi, L., Viceconti, M., 2014. A new
568 paradigm for the in vitro simulation of sideways fall loading of the proximal human
569 femur. Journal of Mechanics in Medicine and Biology 14, 1450005.
570

571

CAPTIONS TO FIGURES:

Fig. 1 - Schematic of a right femur with the position of the strain gauges: medial and posterior views. The levels where strain gauges were placed were defined as a fraction of the femur dimensions (biomechanical length, BL; head diameter, HD). The placement around the head and neck of the strain gauges AH, AN, PH and PN corresponded to the mid-thickness of the neck at the corresponding level. The placement around the head and neck of strain gauges MH, MN, LH and LN corresponded to the intersection of the frontal plane with the cortical surface. The placement around the diaphysis of strain gauges A1, L1, P1, M1, A3, L3, P3 and M3 corresponded to the mid-thickness of the diaphysis at the corresponding level

Reproduced with permission (Copyright of the "Virtual Physiological Osteoporotic Human Project – VPHOP" consortium, http://www.vphop.eu/).

Fig. 2 – Setup to simulate a range of physiological loading directions. LEFT: Schematic of a right femur (anterior and lateral views) showing the direction of the hip joint force for the different loading configurations: LC1 to LC4 covered the extreme directions of the hip joint resultant force in the sagittal and frontal planes; for LC5 the force was applied parallel to the femoral diaphysis; LC6 replicated the case used in destructive tests (Cristofolini et al.,2009). RIGHT: Experimental set-up including the femur specimen, the actuator of the testing machine with the system of linear bearings to avoid transmission of horizontal forces; the femur was potted in acrylic cement distally; interchangeable wedges were used to achieve the desired loading angles; the applied force was measured by the load cell of the testing machine

Reproduced with permission (Copyright of the "Virtual Physiological Osteoporotic Human Project – VPHOP" consortium, http://www.vphop.eu/).

Fig. 3 - Setup to simulate the sideways fall loading configurations. LEFT: Overview of the loading setup. The femur (a right specimen in this instance) was held through its distal pot. The internal rotation angle could be adjusted distally. The adduction angle was selected adjusting the height of the distal constraint. Thanks to a bearing, the femur was free to tilt about the distal axis. The greater trochanter rested on a flat support, which could slide on linear bearings. The force was applied to the femoral head by the actuator of the testing machine through a system of linear bearings. Load application to the greater trochanter and the femoral head was mediated by two aluminum caps fixed with acrylic cement to avoid local crushing (Zani et al.,2014). RIGHT: Experimental set for the destructive tests: the femur is visible under the testing machine; the high-speed camera was mounted on a tripod, directly facing the superior-lateral part of the neck (except for some specimens where it faced the medial part); two mirrors (only one is visible here) were used so as to reflect the posterior and anterior sides of the femur); the light sources are also visible (Zani et al.,2014), (Cristofolini et al.,2007)). Two LVDTs are also visible near the proximal region of the femur, which were part of a different study simulations(Grassi et al.,2012).

Fig. 4 - Magnitude of the maximum (ε_1) and minimum (ε_2) principal strains (in microstrains) for the 6 different loading configurations covering the physiological range (see Fig. 2). The bars indicate the average and standard deviation between 11 specimens. The significance of the effect of the loading configuration is reported for each strain gauge (ANOVA test).

Fig. 5 - Magnitude of the maximum (ε_1) and minimum (ε_2) principal strains (in microstrains) for the 12 different loading directions explored for a sideways fall (the internal rotation angle, INT, was tested at 0°, 15° and 30°, the adduction, ADD, was tested at 0°, 10°, 20° and 30°, see Fig. 3). The bars indicate the average and standard deviation between 11 specimens. The significance of the effect of the internal rotation and adduction angles are reported for each strain gauge (ANOVA test).

Fig. 6 – Direction of the principal strains for the 6 different loading configurations covering the physiological range (see Fig. 2). For each strain gauge, the angle θ_p of the maximum tensile principal strain is reported in terms of counterclockwise variations with respect to loading configuration LC6 (8° adduction), which was assumed as a reference. An angle close to 0° indicates that the principal strain for that loading configuration was aligned as the reference one (LC6). To enable pooling of all specimens, the angles of the left femurs were mirrored, so that all angles are reported as if we tested only right femurs. The bars indicate the median and standard deviation between 11 specimens. The significance of the effect of the loading configuration is reported for each strain gauge (Kruskal-Wallis test).

Fig. 7 – Direction of the principal strains for the 12 different loading directions explored for a sideways fall (the internal rotation angle, INT, was tested at 0°, 15° and 30°, the adduction, ADD, was tested at 0°, 10°, 20° and 30°, see Fig. 3). For each strain gauge, the angle θ_p of the maximum tensile principal strain is reported in terms of counterclockwise variations with respect to physiological loading configuration LC6 (8° adduction), which was assumed as a reference. An angle close to 90° indicates that the principal strain for that loading configuration was perpendicular to the reference one (LC6). To enable pooling of all specimens, the angles of the left femurs were mirrored, so that all angles are reported as if we tested only right femurs. The bars indicate the median and standard deviation between 11 specimens. The significance of the effect of the internal rotation and adduction angles are reported for each strain gauge (Kruskal-Wallis test).

Fig. 8 - Typical fracture mechanism observed during a sideways fall observed with in the high-speed videos (a left femur, specimen #5). The image in the centre of each picture is a direct view of the femoral neck from the medial side; the ones on the left and right are reflected images (posterior and anterior sides respectively) obtained from the two mirrors placed next to the femur and suitably oriented (Fig. 3). Picture A shows the femur shortly before the first signs of fracture are seen (0.6 ms before Picture B). Picture B shows the instant when compression failure is seen on the superior-lateral side (indicated by the yellow pointers). Picture C (0.4 ms after Picture B) shows the final stage, when tension leads failure on medial side (indicated by the yellow pointers). The pictures have low resolution (1 pixel = approximately 0.2 mm on the physical specimen) because they were acquired by the high-speed camera. Electro-conductive lines are visible on the neck surface, which were part of a different study (Juszczyk et al.,2010; Juszczyk et al.,2013).

Reproduced with permission (Copyright of the "Virtual Physiological Osteoporotic Human Project – VPHOP" consortium, http://www.vphop.eu/).

Fig. 9 - Typical curves during the destructive test: the force and strains are plotted as a function of the actuator displacement. The maximum (ε_1) and minimum (ε_2) principal strains (in microstrains) are reported for all strain gauges. The head, neck, level 1 and level 3 are plotted separately. Specimen #8 is reported here; the plots of the remaining femurs are available with the supplementary material <LINK>.

Reproduced with permission (Copyright of the "Virtual Physiological Osteoporotic Human Project – VPHOP" consortium, http://www.vphop.eu/).

TABLES

Table 1 – Details of the specimens. In the first columns, details of the donors are listed. Biomechanical dimensions (Cristofolini,2012; Ruff and Hayes,1983) are reported in the 8th and 9th columns. Bone quality is reported in the last column (T-score of the bone density, based on the Norland DEXA scanner reference population).

	DONORS' DETAILS					FEMURS' DETAILS			
Femur ID	Gender	Age at death	Cause of death	Donor Height (cm)	Donor Weight (kg)	Side	Biomechanical Length, BL (mm)	Head Diameter, HD (mm)	DEXA T-score
#1	Female	74	Respiratory failure	173	72	Left	390	40.5	0.62
#2	Female	59	Myocardial infarction	152	117	Right	384	45.0	-2.36
#3	Male	65	Myocardial infarction	188	95	Left	479	56.0	-0.50
#4	Female	80	Cerebrovascular accident (CVA)	155	66	Right	384	42.2	-4.07
#5	Female	80	Cerebrovascular accident (CVA)	155	66	Left	387	42.0	-4.05
#6	Male	62	Chronic obstructive pulmonary disease (COPD)	173	131	Right	403	47.2	-3.74 (*)
#7	Male	62	Chronic obstructive pulmonary disease (COPD)	173	131	Left	409	46.8	-1.22 (*)
#8	Female	84	Senile dementia	168	63	Right	418	44.2	-2.68 (*)
#9	Female	84	Senile dementia	168	63	Left	421	44.5	-1.44 (*)
#10	Female	68	Amiotrophic lateral sclerosis	160	63	Right	418	44.2	-2.59 (*)
#11	Female	77	General debility	185	76	Right	411	45.8	-3.74 (*)
MEDIAN	-	74	-	168	72	-	409	44.5	-2.59
SD	-	9.4	-	12	28	-	27	4.1	1.56
RANGE	-	59 - 84	-	152 - 188	63 - 131	-	384 - 479	40.5 - 56.0	-4.07 - 0.62

(*) Note: For the highlighted femurs the DXA scan was not available. The DXA T-score was obtained from CT-data: femoral neck volumetric bone mineral density (vBMD) was calculated by manually selecting a femoral neck region corresponding to that routinely used in DXA, and using the available CT densitometric calibration, obtained through the European Spine Phantom. A simulated T-score was then calculated from vBMD by applying a linear regression obtained on a different set of 20 femora, for which both vBMD from CT and T-score from DXA were available (Taddei et al.,2014).

Table 2 – Details of the destructive tests with a simulated sideways fall. The actuator speed is indicated. The details of the failure event include: peak force (maximum peak recorded during the destructive tests: in absolute terms, and as a fraction of the donors' body weight); vertical displacement of the actuator corresponding to the force peak (Fig. 3); time corresponding to the force peak. A description of the mode of failure is reported.

Femur ID	Actuator speed (mm/sec)	Peak failure force (N)	Peak failure force (BW)	Actuator displacement at force peak (mm)	Time to force peak (seconds)	Description of failure	NOTES
#1	18.0	5160	7.31	3.05	0.17	Two-phase inter-trochanteric fracture	
#2	32.5	2912	2.54	3.42	0.10	Crushing of greater trochanter	
#3	49.5	6529	7.01	6.69	0.13	Two-phase inter-trochanteric fracture	
#4	32.5	2799	4.32	3.33	0.10	Two-phase neck fracture	
#5	15.5	2545	3.93	2.33	0.15	Two-phase neck fracture	
#6	27.5	3406	2.65	2.86	0.10	Crushing of greater trochanter	Very short neck
#7	30.0	2716	2.11	4.03	0.13	Crushing of greater trochanter	Very short neck
#8	17.5	2167	3.51	1.84	0.10	Two-phase sub-capital fracture	
#9	25.0	2842	4.60	2.31	0.09	Two-phase inter-trochanteric fracture	
#10	22.5	2694	4.36	missing	missing	Crushing of greater trochanter	Force-displacement file corrupted
#11	25.0	1170	1.57	missing	missing	Two-phase inter-trochanteric fracture	Force-displacement file corrupted
MEDIAN	25.0	2799	3.93	3.05	0.10		-
SD	9.5	1464	1.85	1.43	0.03		-
RANGE	15.5 - 49.5	1170 - 6529	1.57 - 7.31	1.84 - 6.69	0.09 - 0.17		-

Fig_1
Click here to download high resolution image

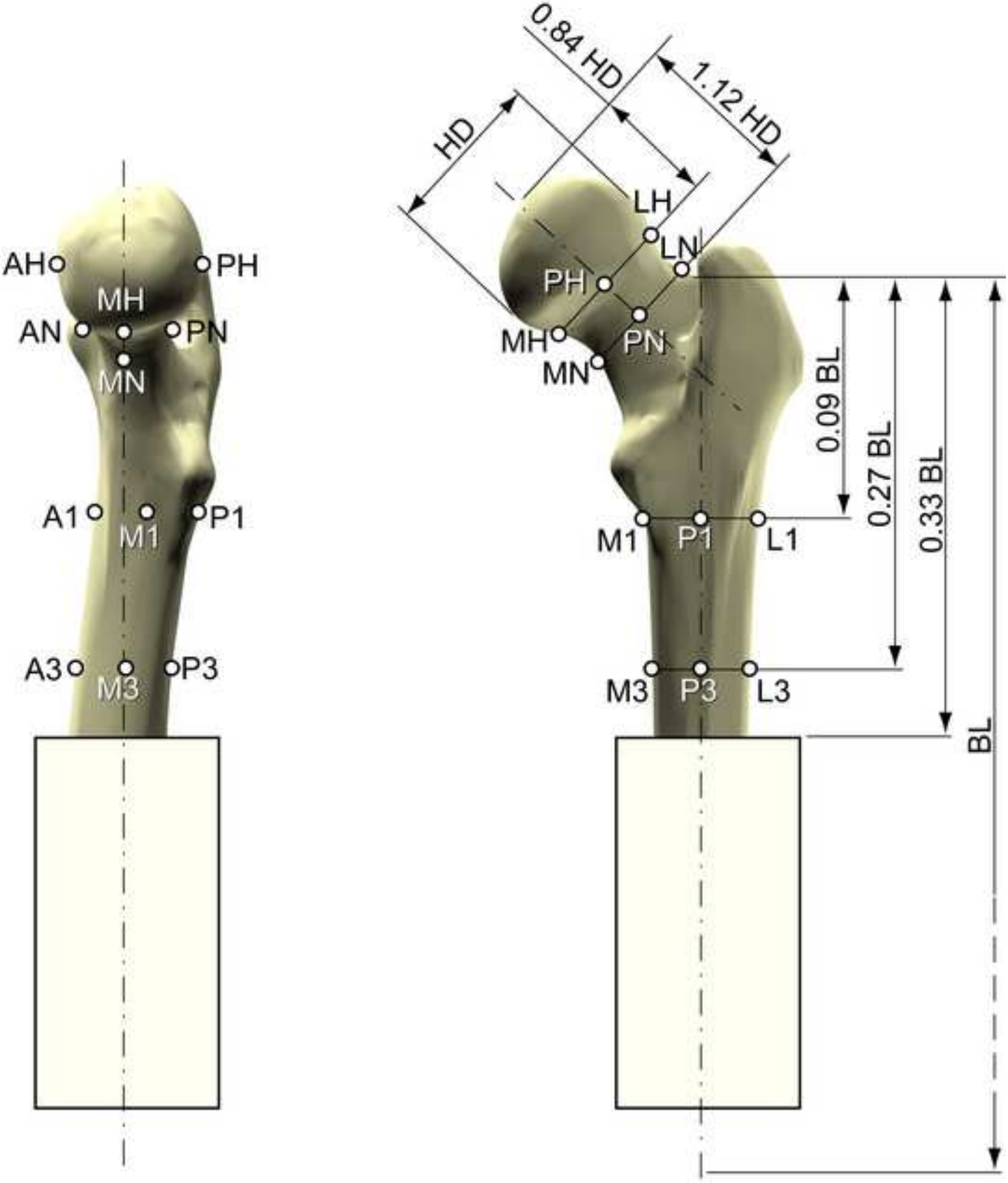

Fig_2

Click here to download high resolution image

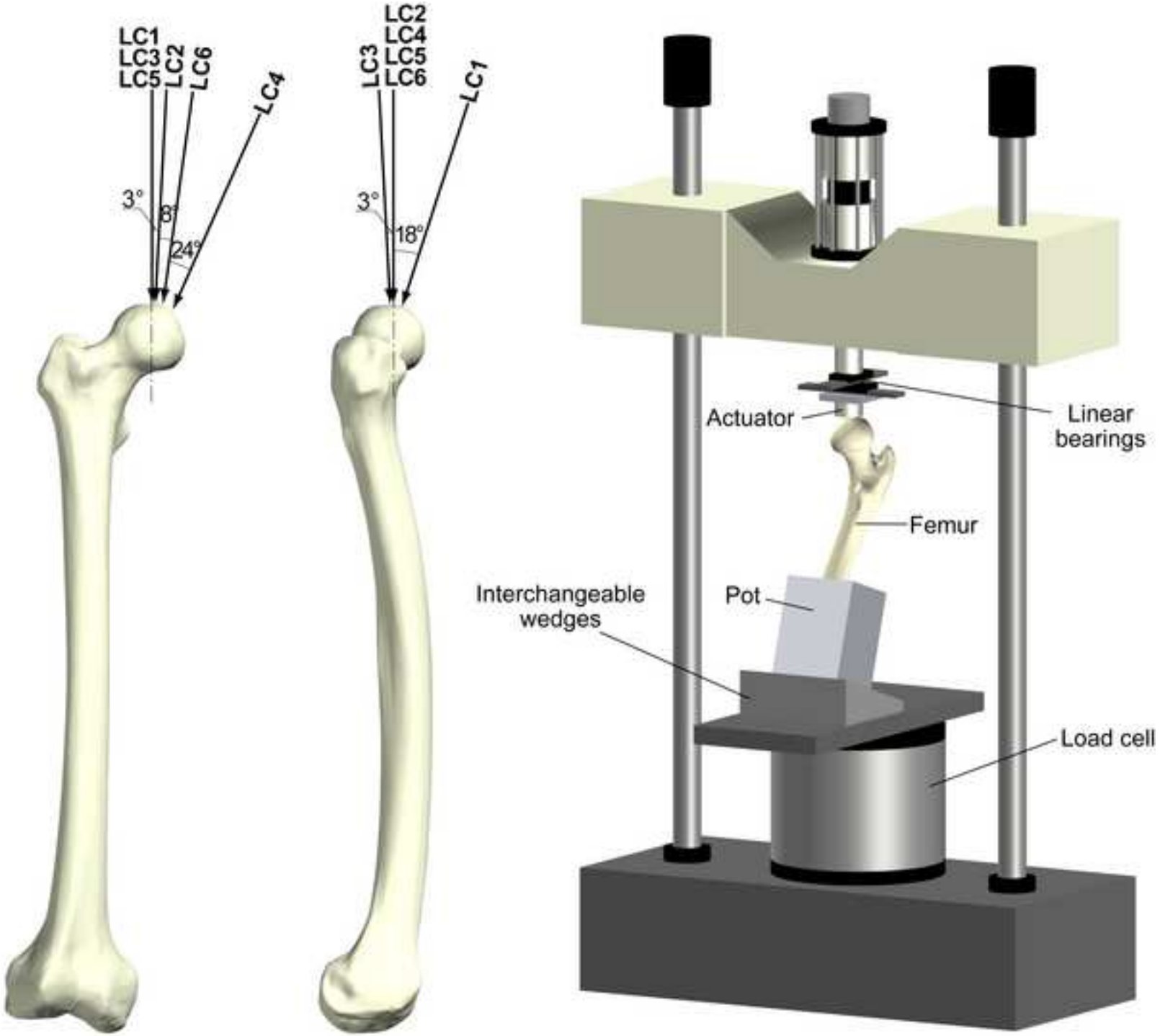

Fig_3
Click here to download high resolution image

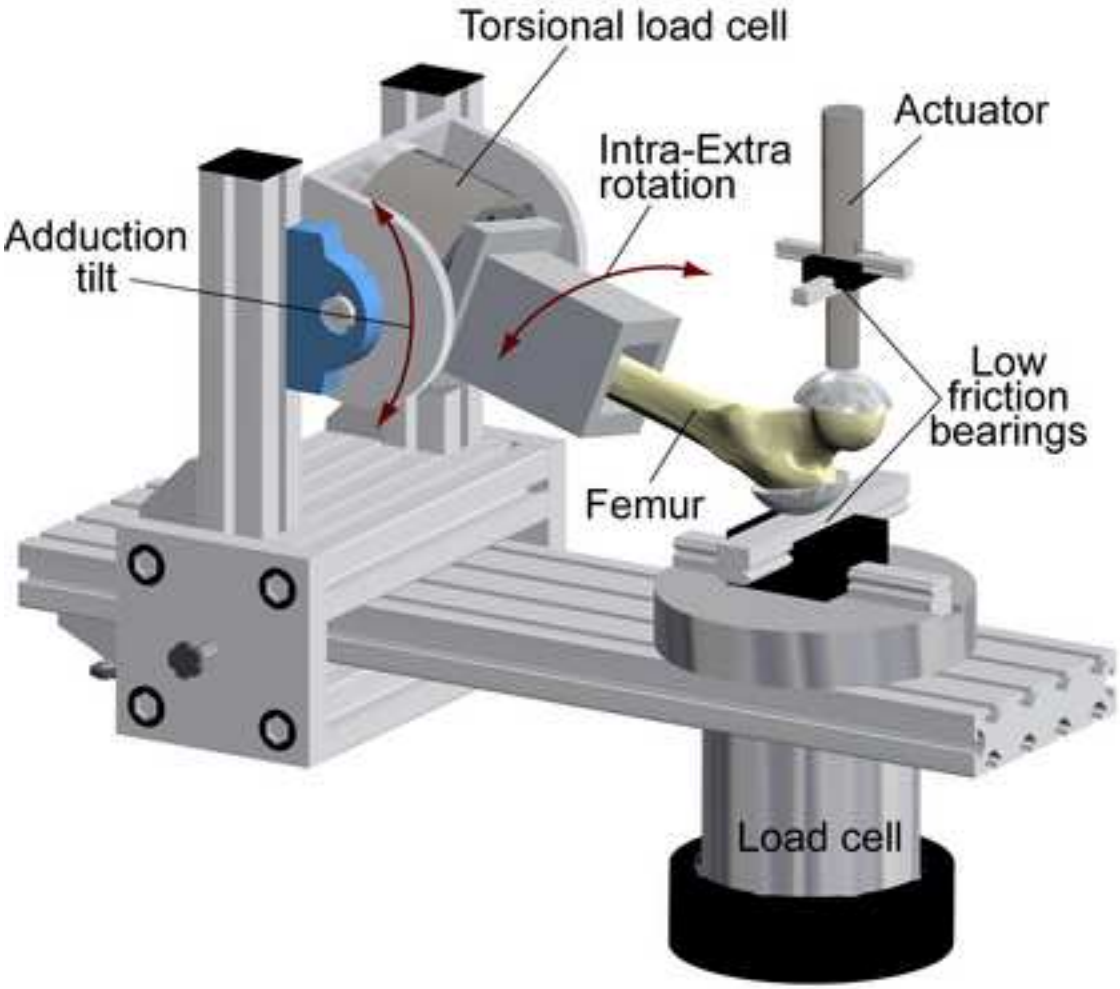

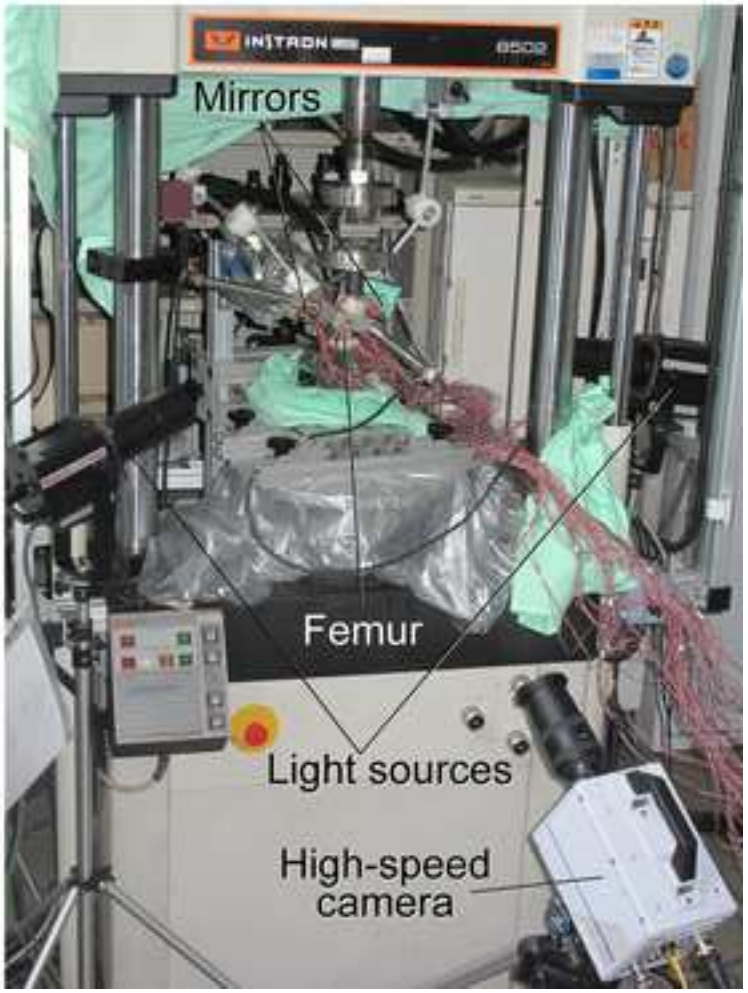

Fig_4

Click here to download high resolution image

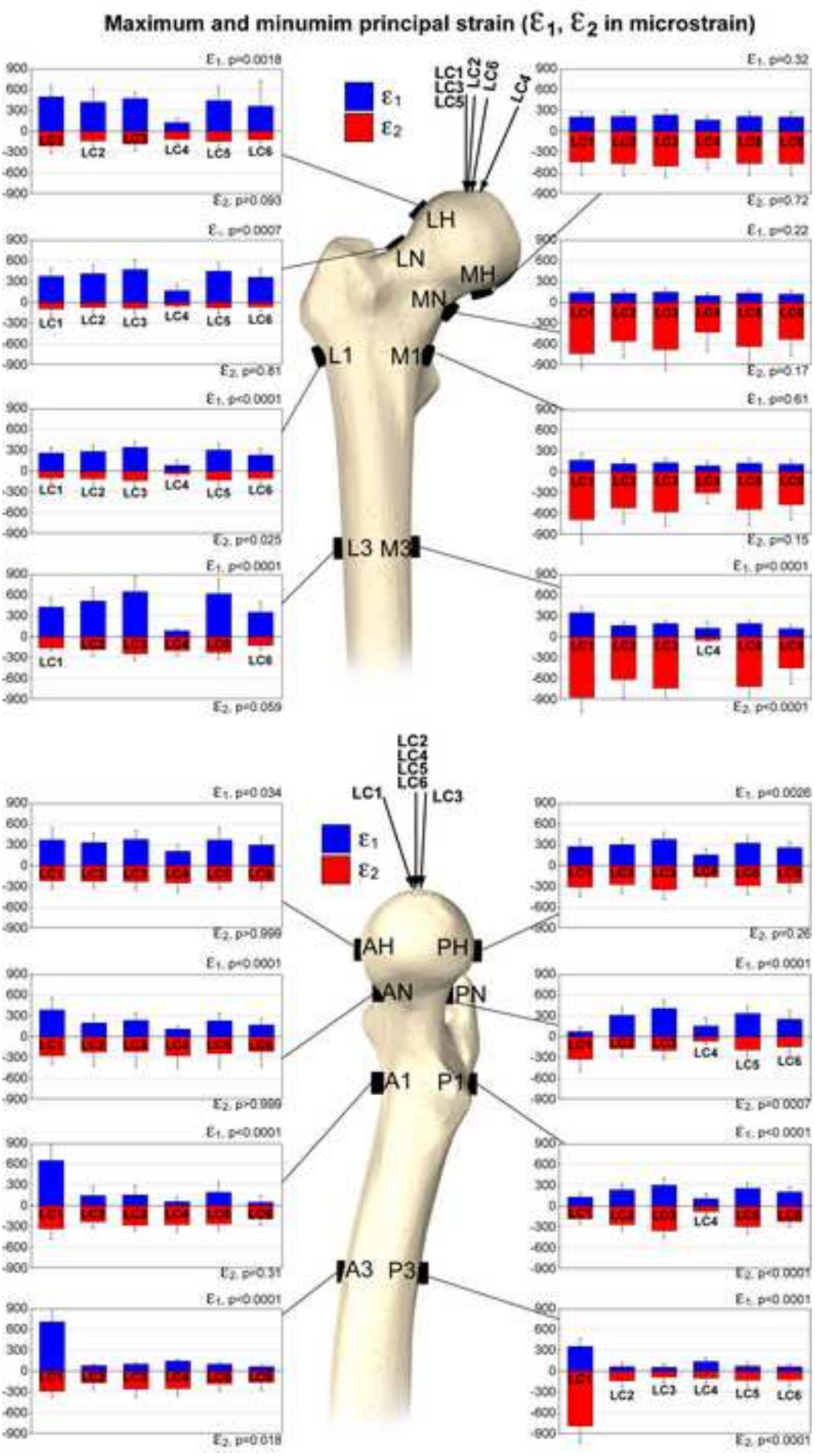

Fig_5

Click here to download high resolution image

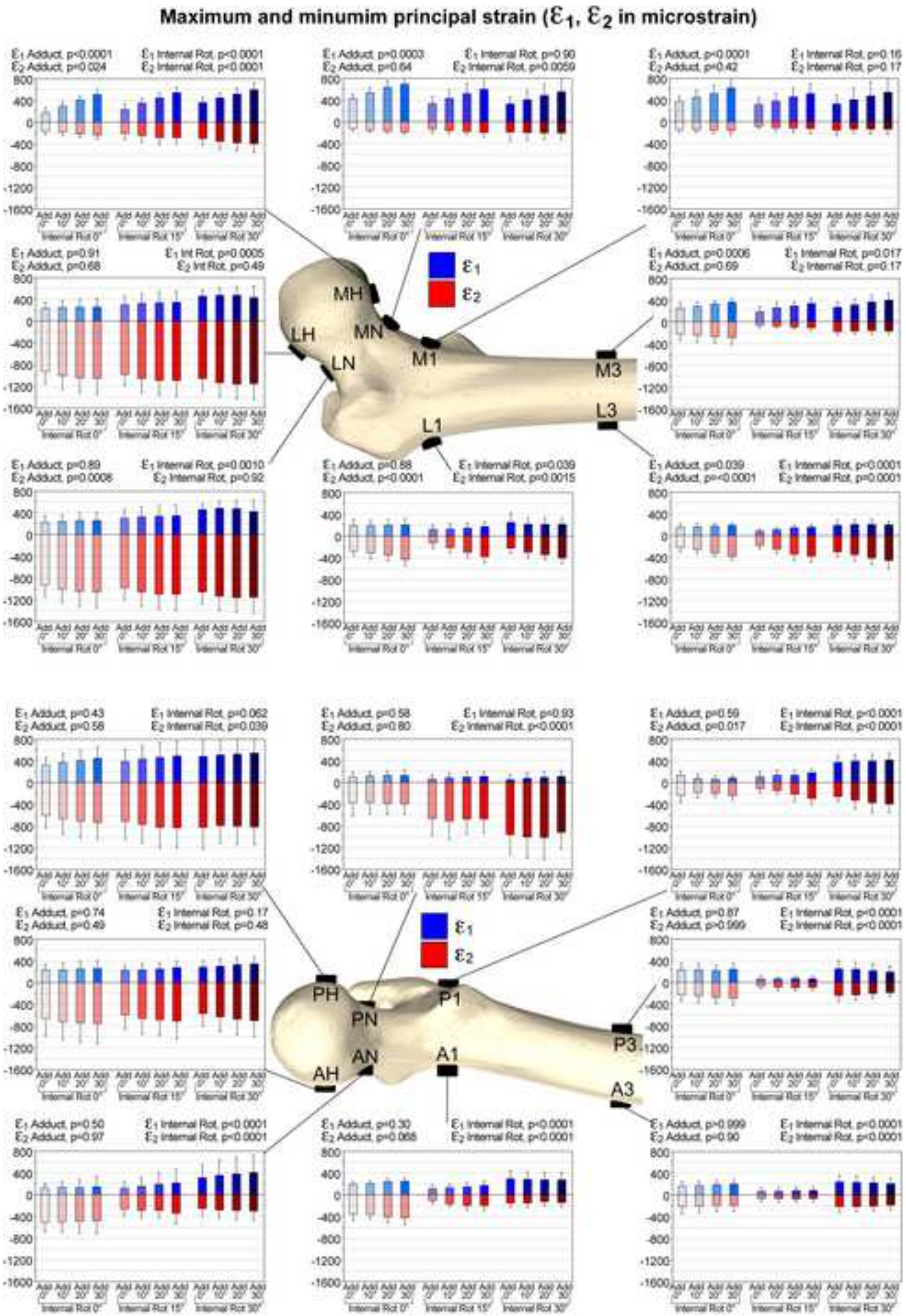

Fig_6

Click here to download high resolution image

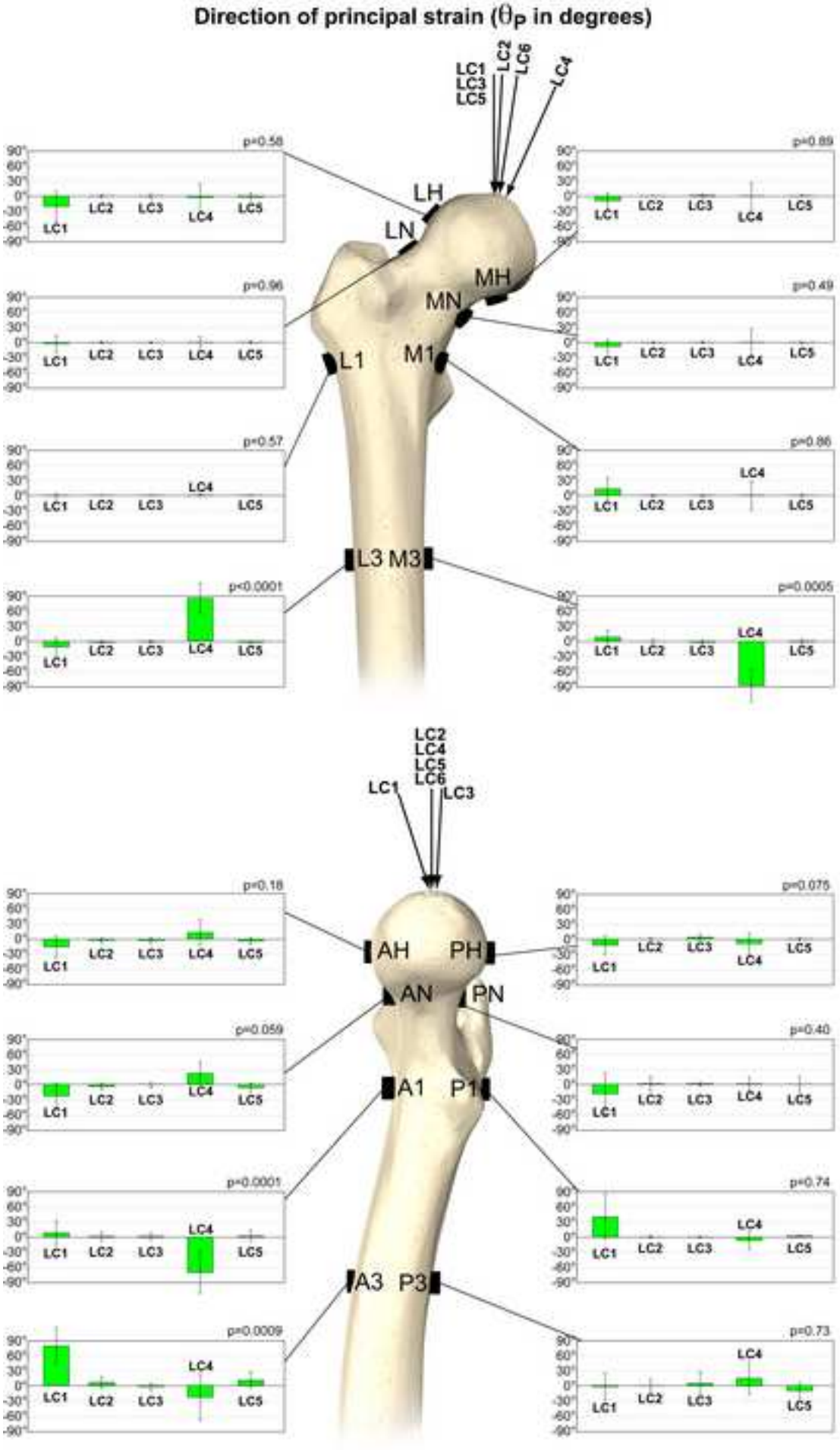

Fig_7

Click here to download high resolution image

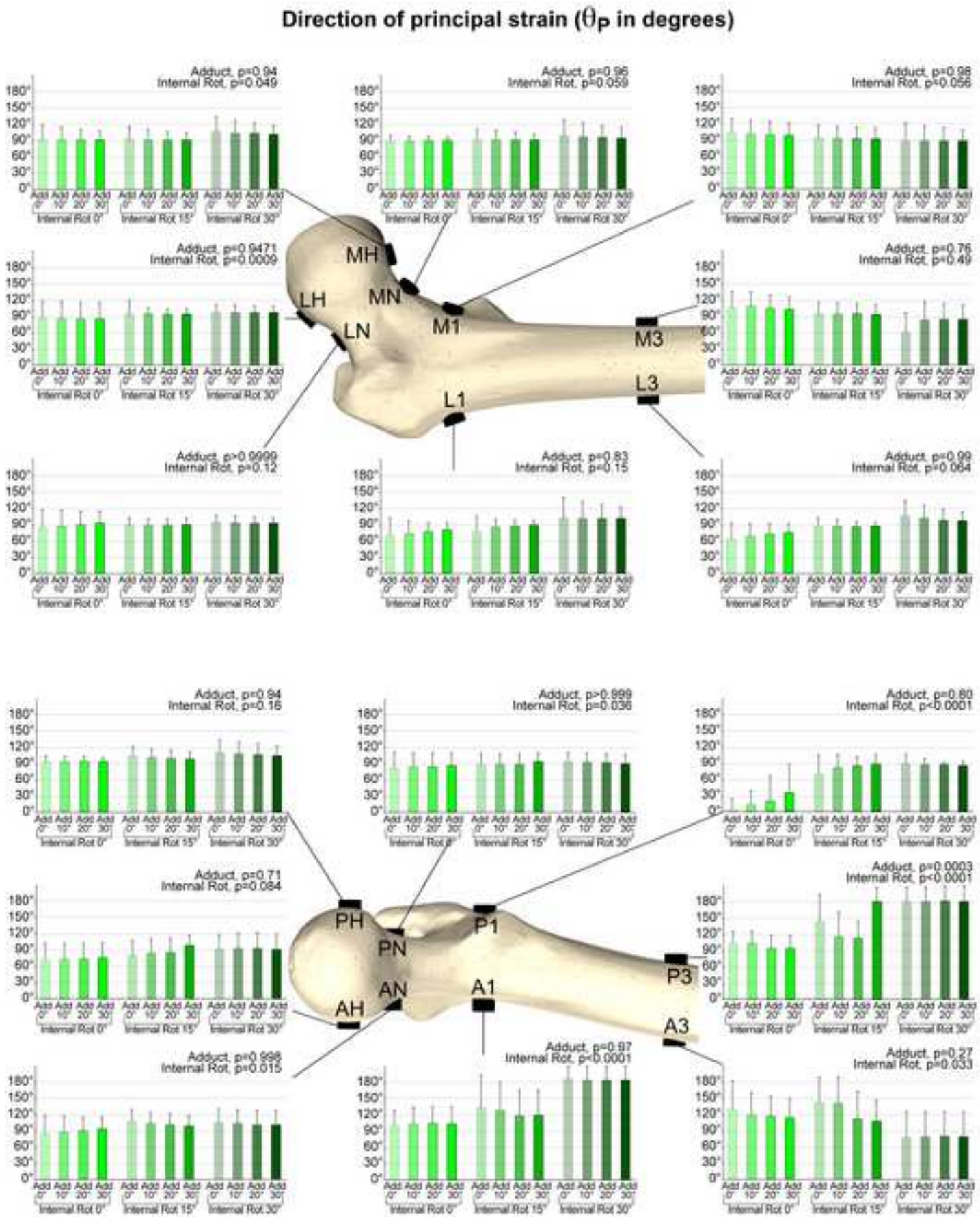

Fig_8
Click here to download high resolution image

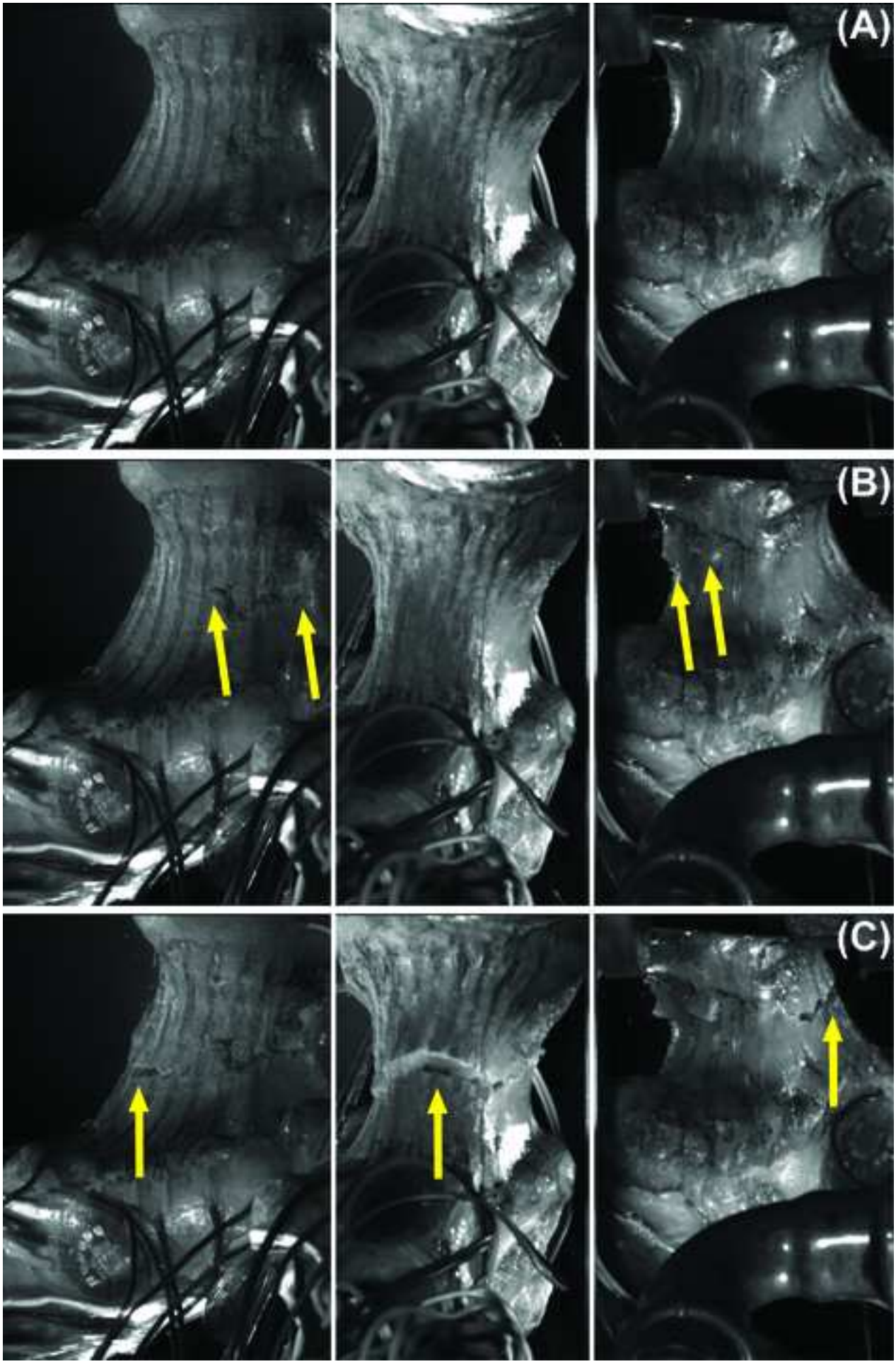

Fig_9

Click here to download high resolution image

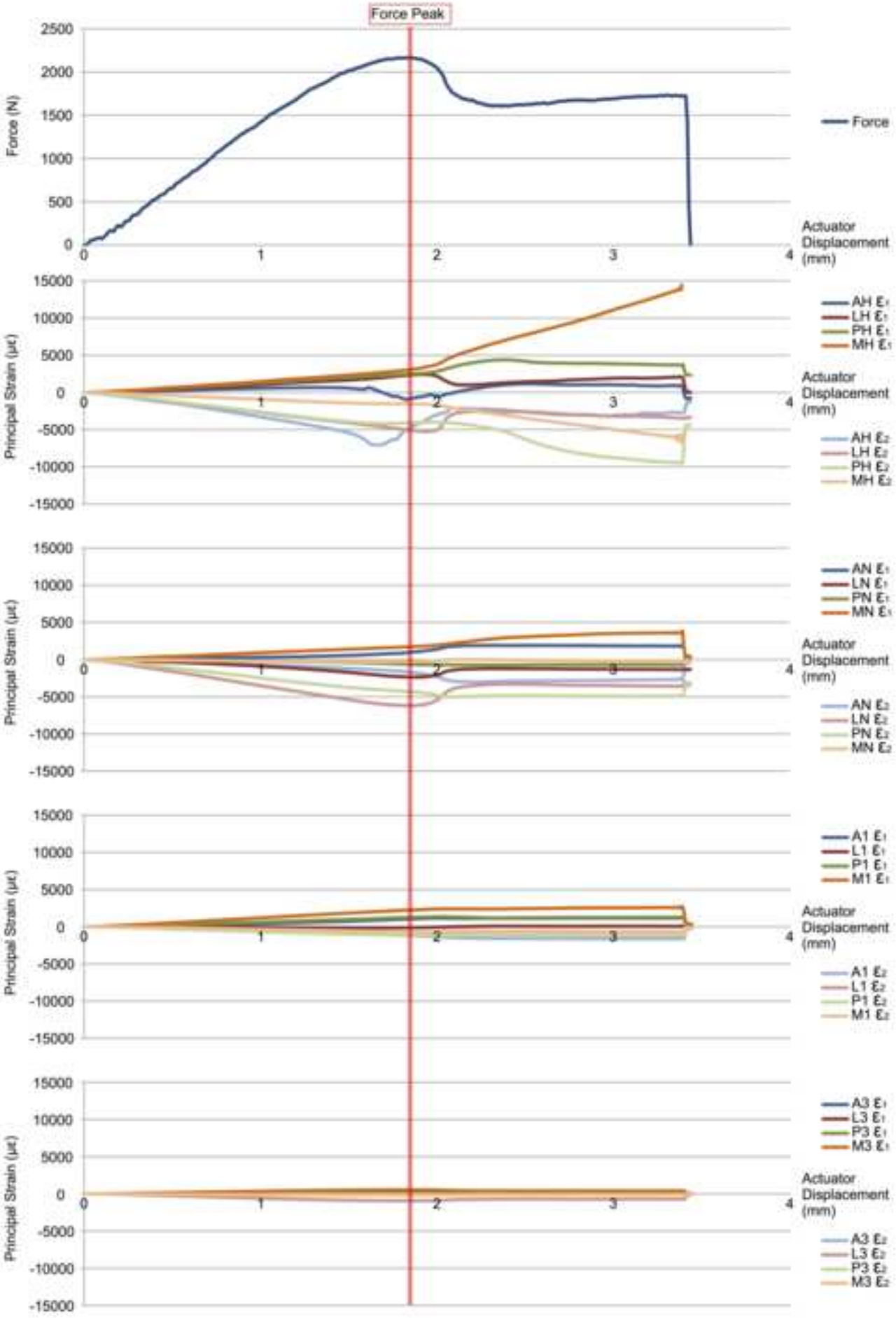

Conflict of interest

There is no potential conflict of interest: none of the Authors received or will receive direct or indirect benefits from third parties for the performance of this study. This study was funded by the European Community Seventh Framework Programme (‘‘The Osteoporotic Virtual Physiological Human—VPHOP’’ Grant FP7- ICT2008-223865, and ‘‘MXL’’, Grant ICT-2009.5.2 248693), and by the Italian Ministry of Education (PRIN 2010-11, Grant 2010R277FT “Fall risk estimation and prevention in the elderly using a quantitative multifactorial approach”).